Optimal Control Surface Mixing of a Rhomboid-Wing Unmanned Aerial Vehicle

E. Miles[1]
University of Pretoria, Pretoria, Gauteng, 0181, South Africa

B.A. Broughton[2]
Incomar Aerospace and Defence Systems, Centurion, Gauteng, 0181, South Africa

This paper describes a method for determining an optimal control allocation function for aircraft with an unconventional control surface setup (i.e. that does not consist of a conventional elevator, rudder and ailerons). A typical application of this control mixing would be to impart conventional handling qualities to an unconventional unmanned aerial vehicle (UAV), which will enable a pilot to fly the UAV manually during flight testing. The mixing can also be used as a backup mode in order to recover the UAV manually, should any sensor failures occur during flight testing. Furthermore, the allocation can be used to simplify the inner control loops of a UAV autopilot or stability augmentation system. The control allocation design process was formulated as a multi-objective optimization problem. A methodology was proposed to define the constraints, which can be customized for a particular aircraft or application.

Nomenclature

$\boldsymbol{A}$	=	Matrix containing quadratic control allocation coefficients (deg)
$\boldsymbol{B}$	=	Matrix containing linear control allocation coefficients (deg)
f	=	Normalized function
$F(\boldsymbol{x}^*)$	=	Objective function solution at optimum point
$\boldsymbol{g(x)}$	=	Inequality constraints
$\boldsymbol{h(x)}$	=	Equality constraints
p	=	Roll rate (deg/s)
$\dot{p}$	=	Roll acceleration (deg/s^2)

[1] Department of Mechanical and Aeronautical Engineering, Private bag X20, Hatfield 0028, South Africa.
[2] Senior Aeronautical Engineer, Incomar Aerospace and Defence Systems, PO Box 68354, Highveld 0169, South Africa.

q = Pitch rate (deg/s)

$\dot{q}$ = Pitch acceleration (deg/s^2)

r = Yaw rate (deg/s)

$\dot{r}$ = Yaw acceleration (deg/s^2)

r_p = pitch command (normalized -1 to 1)

r_r = roll command (normalized -1 to 1)

r_y = yaw command (normalized -1 to 1)

$\boldsymbol{T}$ = Trim bias vector (deg)

V_T = True airspeed (m/s)

$\dot{V_T}$ = Airspeed derivative (m/s^2)

w = Objective function term weight

$\boldsymbol{x}$ = Optimization design vector

α = Angle of attack (deg)

$\dot{\alpha}$ = Angle of attack acceleration (deg/s)

β = Sideslip angle (deg)

$\dot{\beta}$ = Sideslip angle acceleration (deg/s)

δ_i = Deflection of control surface i (deg)

δ_{throttle} = Throttle position

I. Introduction

THE unmanned aerial vehicle (UAV) sector is one of the fastest growing sectors in the aerospace industry. Various resources are being invested into the further development of new technologies and low-cost UAVs that can provide low-risk solutions to numerous requirements. Due to increased demands on aircraft performance and efficiency, and the fact that UAVs often do not have to comply with many of the requirements that drive manned aircraft towards relatively conventional layouts, UAVs often make use of unconventional configurations. It is also common to find redundant control surfaces on UAVs to improve their robustness. The aircraft used to demonstrate the methodology described in this paper made use of a Rhomboid wing configuration which is shown in Fig 1. A rhomboid-wing configuration is a type of joined-wing [1] concept where the two forward wings are swept back, while the two rear wings are swept forward, the wing tips of this configuration are interconnected which also leads

to the term box-wing aircraft. The fundamentals of this unconventional airframe are discussed in [2], with a typical conceptual design process of such an airframe discussed in [3]. Quite extensive research has been conducted on joined-wing aircraft by the USAF [4], papers published such as [5], with further collaborations between NASA and Boeing on highly nonplanar lifting systems [6].

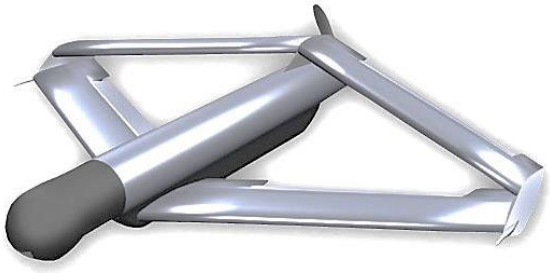

Fig 1 Paramount Advance Technologies Roadrunner UAV

The UAV configuration utilized in this paper was configured with eight control surfaces, none of which were located on a vertical surface such as a conventional rudder. Although roll and pitch control could potentially be assigned using an intuitive approach, yaw control poses a particular challenge. The assignment of the different control surfaces were further complicated by a requirement to somewhat decouple roll, pitch and yaw responses in order to provide a response that resembled that of a conventional aircraft.

Despite the obvious challenges in utilizing the control surfaces of this configuration effectively, the natural stability characteristics of the airframe were found to be relatively conventional. By placing the center of gravity ahead of the neutral point, conventional static stability could be ensured and initial flight tests as a simple radio controlled model demonstrated conventional longitudinal dynamic response modes. The wind tunnel data and subsequent work conducted on this project demonstrated that significant tailoring of the response was possible. For example, it was possible to slightly influence the apparent dihedral effect by mixing the control surfaces appropriately, and adverse yaw could be adjusted or eliminated as desired. Dutch roll behavior appeared to be conventional, although somewhat lightly damped. One particular challenge, as expected and confirmed by the wind tunnel data, was that none of the control surfaces could really generate a large yawing moment especially for small control surface deflections. This characteristic made the assignment of control surfaces for yaw control even more difficult than initially anticipated.

There have been numerous studies on efficient and optimal control allocation such as the study by Zhang, Suresh, Jiang and Theilliol [7] who investigated the use of an unconventional control surface setup in an optimal

way. The aim of the study by Zhang *et al.* was to develop a control allocation function that could reallocate controls in the case of an aircraft control effector failure. Furthermore, Doman and Oppenheimer assisted Poonamallee, Yurkovich and Serrani [8] to develop a nonlinear control allocation method by using the linear control allocation developed in [9] as a basis. The aim of the study by Doman *et al.* was to compare the performance of the nonlinear control allocation function to other control allocation approaches.

Some of the studies discussed above had an open-loop allocation component, but it was mostly used as a starting point for the closed-loop feedback design. Many other researchers have also investigated related topics, such as fault-tolerant control [10], adaptive control [11] and fuzzy logic control [12] systems. The control allocation strategy developed in this paper differs from previous studies in that the focus of the current study was on the open-loop control allocation problem, whether as a "flight test" or "backup" mode, or when used in the inner control loops of a feedback control or stability augmentation system.

II. Modelling and Simulation

The control allocation design process required an accurate, nonlinear, six degree-of-freedom model of the aircraft that could be implemented in a simulation environment. A custom six degree of freedom simulation environment was utilized that was particularly flexible in the different types of steady-state conditions (trim states) that could be specified. It could also simulate the response of the aircraft to control inputs utilizing a conventional fourth order Runge-Kutta integration scheme [13]. The simulation environment was populated with a model of the UAV that was developed from a combination of wind tunnel data, analytical and numerical predictions and mass and inertia measurements of the actual test airframe. A separate propulsion model was also developed to predict the forces and moments generated by the electric motor/propeller combination. Torque and gyroscopic effects were taken into account, which resulted in asymmetric responses even though the airframe was geometrically symmetric.

A. Wind tunnel tests

A wind tunnel test series was conducted at the Council for Scientific and Industrial Research (CSIR) in South Africa that preceded the current study [14]. These tests were performed using a full-scale model of the aircraft in the CSIR low-speed wind tunnel. The airframe characterization tests were executed by using the Modern Design of Experiments (MDOE) technique [15], [16]. MDOE is aimed at extracting as much information as possible from a limited number of tests [16]. Characteristic response surfaces were derived in the form of mathematical models that

were statistically defensible. To determine the response surfaces characterizing the airframe, the MDOE technique was used as a function of 10 factors, namely angle of attack, angle of sideslip and the deflections of the eight individual control surfaces. The commercially available package Design-Expert®, from Stat-Ease, was used to analyze the test data [14]. The wind tunnel MDOE tests provided both the static coefficients and the first order control and stability derivatives of the airframe [14].

The MDOE models for the various aerodynamic forces and moments were provided in the form of coefficients of polynomial expressions. The design space was divided into three angle-of-attack ranges, which resulted in separate MDOE models that were valid over each individual range. The low angle of attack region spanned $-6° \leq \alpha \leq 6°$, the high angle of attack region spanned $4° \leq \alpha \leq 11°$ and the post-stall region spanned $14° \leq \alpha \leq 18°$. The design test envelope for the angle-of-attack range therefore covered the range $-6° \leq \alpha \leq 18°$ so that the combined MDOE model was defined over the same range. The sideslip design test envelope consisted of a range of $-10° \leq \beta \leq 10°$.

The low angle of attack and high angle of attack range MDOE models were expressed as second-order polynomials with pure third-order terms, whereas the post-stall region was reduced to a linear model with two additional squared terms. Several asymmetric terms were detected in the MDOE models, which – although statistically significant – were undesirable for the flight dynamics modelling of the physically symmetrical airframe. The MDOE models were therefore modified for implementation in the simulation environment by eliminating the asymmetries that resulted from the experimental testing and MDOE analysis technique. Further modification involved taking the average weighted effect of the corresponding control surfaces on the left and right to ensure a perfectly symmetrical modelled aircraft. The corresponding control surfaces are illustrated in Fig 2.

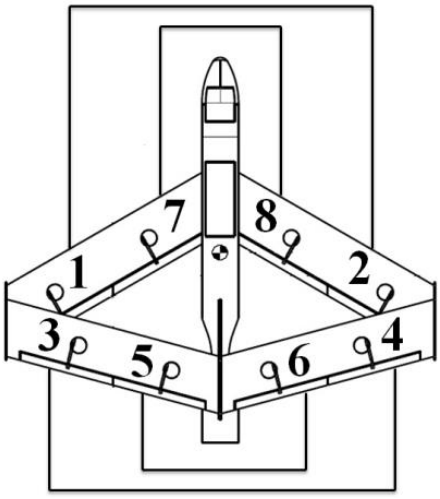

Fig 2 Corresponding control surfaces

In addition, the low, medium and high angle-of-attack aerodynamic models were combined into a single model using blending functions over the overlapping angles of attack (between the low and high angle-of-attack regions) and to span the range from eleven to fourteen degrees angle of attack, which was not covered by the MDOE models at all. The final model gave each of the six body-axis static aerodynamic coefficients as functions of angle of attack, angle of sideslip and a combination of deflections of the eight control surfaces. The entire wind tunnel test series was conducted at 30 m/s and Reynolds number was therefore not included as an independent variable.

The blending functions used were interpolating functions that agreed exactly with the wind tunnel models where those models were defined, and assumed a smooth transition between the separate regions. The three sets of polynomials for the low, high and post-stall angle-of-attack regions were respectively joined together smoothly for all the force and moment MDOE models. Further adjustments were made in some areas to eliminate sudden changes in the gradients.

B. Stability derivatives

The wind tunnel data provided good estimates of the static coefficients, their first derivatives and the control derivatives. Those stability derivatives that were not obtained through the wind tunnel tests were calculated using Athena Vortex Lattice (AVL) [17]. AVL is a software package developed at Massachusetts Institute of Technology (MIT) that is suitable for the aerodynamic and flight-dynamic analysis of rigid aircraft in inviscid, incompressible flow. Although more sophisticated methods could be used, those methods were not deemed necessary for the context of this research as the optimization problem focused on initial angular accelerations and steady-state

conditions, where the damping derivatives would not play a large role. In order to verify the AVL model, static coefficients predicted by the AVL model were initially compared to the wind tunnel results in the low angle of attack range. Despite the expected differences related to the use of a vortex lattice program, correspondence between the AVL and the wind tunnel results on the static coefficients were considered of sufficient accuracy to justify the use of the damping derivatives predicted by AVL in the simulation. Due to difficulties in capturing the side-force and yawing moment coefficient contributions of the fuselage accurately in AVL, additional empirical calculations were used to further augment the dynamic derivatives.

III. Control allocation

The rhomboid UAV utilized in this study used eight control surfaces, of which any individual control surface could contribute to pitch, roll and yaw. Due to these coupled responses, it served as an ideal platform to demonstrate the current technique. The design problem resulting from this aircraft was therefore to allocate the eight control surfaces to provide aircraft responses similar to those expected from conventional elevators, ailerons and rudders.

A. Mixing function

The purpose of the mixing function was to transform the conventional roll, pitch and yaw commands into the required physical deflections of each of the eight control surfaces. The input command vector $[r_p, r_r, r_y]'$ represents the pitch, roll and yaw input commands. These commands were normalised to the range -1 to 1. For example, a roll input $r_r = -1$ represented a full left-roll command, while $r_r = 1$ represented a full right-roll command. A nose-up pitch command is represented by $r_p = 1$, and nose-down by $r_p = -1$. A nose-left-yaw command is represented by $r_y = -1$, and a nose-right–yaw command by $r_y = 1$. The control convention illustrating the pitch command explanation is given in Fig 3. The convention used in this study was that a positive control deflection was one where the trailing edge of the control surface moved downwards.

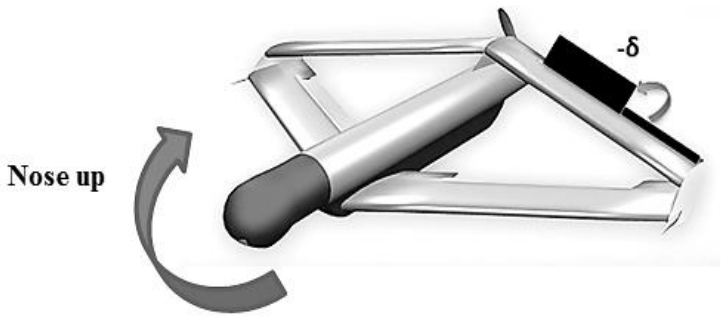

Fig 3 Control surface deflection for a nose-up pitching command

A few control allocation requirements were considered when designing the mixing function. The aim was to design a mixing function with the following capabilities:

- A bias term was required to capture the nominal trim deflections.
- Linear and quadratic terms were required to provide maximum flexibility in the allocation, including left/right control differential.

With regard to the first requirement mentioned above, the objective was to map the zero input case (no pitch, roll or yaw command) to a nominal trimmed aircraft state. Since the mixing function determines the physical control surface deflections (δ), it requires a constant vector, which will be referred to as the 'trim bias vector' (***T***). The trim bias vector for the UAV would therefore contain the eight control surface deflection angles that would initialize the aircraft in a trimmed state. The solution strategy to determine the trim bias vector and matrices ***A*** and ***B*** will be discussed in the next section. The mixing function, consisting of the trim bias vector, the linear term and the quadratic term, is expressed in Equation 1.

$$[\boldsymbol{\delta}] = [\boldsymbol{A}]\begin{bmatrix} r_p{}^2 \\ r_r{}^2 \\ r_y{}^2 \end{bmatrix} + [\boldsymbol{B}]\begin{bmatrix} r_p \\ r_r \\ r_y \end{bmatrix} + [\boldsymbol{T}] \tag{1}$$

The optimization process was separated into two phases. The first objective was to initialize the aircraft in a trimmed state. Since the input commands were, by definition, all zero for the trimmed case, the bias vector could be solved independently. The purpose of the second optimization phase was to obtain the coefficients contained in the ***A*** and ***B*** matrices, which would ultimately allocate the controls for maneuvering and steady states other than the nominal trim condition. The complex and often conflicting mixing requirements necessitated the use of constrained

mathematical optimization throughout the design process. The optimization problem for the two phases is described below.

B. Optimization phase 1: Trim variables

Phase 1 consisted of determining the trim bias vector for a specific steady-state flight condition. The optimization objective for this phase was to obtain the eight control surface deflections that would trim the aircraft, while requiring the individual deflections to deviate as little as possible from the neutral control positions. There were eleven unknowns that had to be solved in order to trim the aircraft: the eight control surface positions, throttle position (δ_{throttle}), angle of attack (α) and sideslip angle (β). The eleven unknowns forming the design vector are given in Equation 2.

$$\boldsymbol{x} = [\delta_1, \delta_2, \delta_3, \delta_4, \delta_5, \delta_6, \delta_7, \delta_8, \delta_{\text{throttle}}, \alpha, \beta] \tag{2}$$

In order to minimize each control surface's deviation from the neutral position, the objective function was defined as the sum of the squares of the control surface positions, as shown in Equation 3. The reader is reminded that a neutral position corresponds to a deflection of zero degrees, as per the convention used in this paper.

$$\boldsymbol{f}(\boldsymbol{x}) = \sum_{i=1}^{6} [\delta_i{}^2] \tag{3}$$

The final step in the formulation process for phase 1 was to identify all the constraints placed on the design. Aircraft trim was enforced through six equality constraints. These constraints were: Roll acceleration ($\dot{p}$), yaw acceleration ($\dot{r}$), pitch acceleration ($\dot{q}$), angle-of-attack acceleration ($\dot{\alpha}$), sideslip-angle acceleration ($\dot{\beta}$) and the speed derivative ($\dot{V}_T$) – which were all required to be zero. The equality constraint vector is mathematically expressed below:

$$\boldsymbol{h}(\boldsymbol{x}) = [\dot{p}, \dot{r}, \dot{q}, \dot{\alpha}, \dot{\beta}, \dot{V}_T] = \boldsymbol{0} \tag{4}$$

C. Optimization phase 2: Control surface mixing variables

The purpose of the second optimization phase was to find the optimal mixing coefficient matrices $\boldsymbol{A}$ and $\boldsymbol{B}$. The optimization objective for this phase was to maximize the aircraft response in all three axes. The design variables in Phase 2 were the coefficients contained in the mixing matrices $\boldsymbol{A}$ and $\boldsymbol{B}$. The eight control surfaces and three input commands resulted in an 8 x 3 matrix. The aircraft was geometrically symmetrical, but due to gyroscopic effects of

the propeller could not be assumed to be "aerodynamically" symmetrical. Nevertheless, symmetry was imposed in the control allocation (not including the trim bias vector), to reduce the number of design variables. This symmetry implied that the control deflections for a left input command in yaw or roll would mirror the control deflections for a right yaw or roll command.

By utilizing "mirrored" design variables in the coefficient matrix, the optimization problem was reduced to 24 design variables in Phase 2 instead of the 48 that would be required if symmetry was ignored. Mixing matrix $\boldsymbol{A}$ contained the first 12 design variables, as shown in Equation 5, and mixing matrix $\boldsymbol{B}$ contained the remaining 12 design variables, as shown in Equation 6. The negative signs in matrix $\boldsymbol{B}$ followed from the anti-symmetric control deflections that are normally associated with roll and yaw commands.

$$\boldsymbol{A} = \begin{bmatrix} x_1 & x_2 & x_3 \\ x_1 & x_2 & x_3 \\ x_4 & x_5 & x_6 \\ x_4 & x_5 & x_6 \\ x_7 & x_8 & x_9 \\ x_7 & x_8 & x_9 \\ x_{10} & x_{11} & x_{12} \\ x_{10} & x_{11} & x_{12} \end{bmatrix} \tag{5}$$

$$\boldsymbol{B} = \begin{bmatrix} x_{13} & x_{14} & x_{15} \\ x_{13} & -x_{14} & -x_{15} \\ x_{16} & x_{17} & x_{18} \\ x_{16} & -x_{17} & -x_{18} \\ x_{19} & x_{20} & x_{21} \\ x_{19} & -x_{20} & -x_{21} \\ x_{22} & x_{23} & x_{24} \\ x_{22} & -x_{23} & -x_{24} \end{bmatrix} \tag{6}$$

The objective for Phase 2 was to maximize the aircraft response in all three axes (lateral, directional and longitudinal). In particular, the responses utilized in the objective function (Equation 7) were selected based on the way in which an aircraft is usually flown: Pitch and roll control are used as the primary inputs for maneuvering an aircraft, while yaw control is usually utilized to balance the aircraft by reducing sideslip or lateral acceleration. Correspondingly, the initial pitch and roll accelerations due to individual roll and pitch commands were selected to be maximized. Furthermore, it was decided to maximize the sideslip angle that could be generated by a yaw command in order to ensure that the aircraft could be balanced while maneuvering. It should be pointed out that alternative formulations can also be used. A scalarized multiple-objective optimization formulation was used, which consisted of multiple objectives placed in one objective function where they were related by weightings.

$$f(\boldsymbol{x}) = -(2w_1\dot{p}_{\text{cond1}} + w_3\dot{q}_{\text{cond3}}) + (2w_2\beta_{\text{cond2}} + w_4\dot{q}_{\text{cond4}}) \quad (7)$$

In the objective function, $\dot{p}_{\text{cond1}}$ was the initial roll acceleration resulting from a maximum roll control input, β_{cond2} represented the steady-state sideslip generated by a maximum yaw control input, $\dot{q}_{\text{cond3}}$ was the initial pitch acceleration for a maximum positive pitch input (nose up) and $\dot{q}_{\text{cond4}}$ for a maximum negative pitch input (nose down). The first condition required a full roll input command to the simulation to obtain the maximum achievable roll acceleration, while the pitch and yaw commands remained zero (r_r = 1, r_p = 0, r_y = 0). The second condition placed the aircraft in a steady-state sideslip condition using a solver implemented in the trim module of the simulation with a full yaw command as input (r_r = 0, r_p = 0, r_y = 1). The third condition required a full positive pitch command in order to obtain the maximum achievable pitch acceleration, while the roll and yaw input commands remained zero (r_r = 0, r_p = 1, r_y = 0). The fourth condition consisted of a full negative pitch command to obtain the maximum achievable negative (or nose-down) pitch acceleration, while the roll and yaw input commands remained zero (r_r = 0, r_p = -1, r_y = 0).

The factor 2 for the roll and yaw cases in the objective function was used to represent the left and right yaw and roll cases simultaneously (their responses were assumed to be symmetrical, except for the small difference made by the torque of the propeller). The responses obtained for a nose-up pitch command and a nose-down pitch command had different requirements and was therefore evaluated separately. The importance of each objective is reflected by the weights (w) in Equation 7 and the negative sign outside the brackets before the objective function was used to convert the maximization problem into a minimization problem, as required by the optimization program.

In the second phase, equality constraints were imposed to decouple the initial responses to each separate command. The goal was to minimize the secondary effects such as adverse yaw and control coupling, which were undesirable. The equality constraints consisted of two parts: The purpose of the first part was to minimize the pitch and side-slip coupling due to a roll command. Although these equality constraints were able to minimize the initial secondary responses that result from roll inputs, they were not expected to control the longer-term responses that would normally require a feedback control system to eliminate completely (for example, long-term dihedral effect). The first two equality constraints are described below in equations (8) and (9):

$$h_1 = \beta_{\text{cond1}} \tag{8}$$

$$h_2 = \dot{q}_{\text{cond2}} \tag{9}$$

Where $\beta_{\text{cond1}}$is the sideslip achieved after 0.5 seconds following a step roll input command, and $\dot{q}_{\text{cond2}}$ is the pitch acceleration achieved after 0.5 seconds following a step roll input command.

The purpose of the second part was to minimize the pitch and roll coupling for a maximum yaw command. The associated equality constraints are listed below as equations (10) and (11):

$$h_3 = \dot{p}_{\text{cond3}} \tag{10}$$

$$h_4 = \dot{q}_{\text{cond4}} \tag{11}$$

Where $\dot{p}_{\text{cond3}}$ is the roll acceleration achieved after one second following a step yaw input command, and $\dot{q}_{\text{cond4}}$ is the pitch acceleration achieved after one second following a step yaw input command.

The control surface deflections were constrained by considering all the possible command combinations that could be given to this UAV. If the control surface deflections were restricted for every possible input command combination, it would include unnecessary strict constraints, which would result in reduced aircraft performance. The realistic input command combinations that were applicable or that could be encountered during the application of the aircraft were considered and mathematically expressed as inequality constraints. The possible input combinations that were considered are discussed below. It should be noted that the final selection would probably be specific to each individual application.

This particular UAV was designed to operate in a surveillance role and the input command combinations were thus assessed according to those types of missions. There were 26 combinations of inputs that contained maximum values of one or more of the commands. The 26 command combinations are listed in Table 1. The first column is a case identifier, while the second, third and fourth columns contain the possible pitch, roll and yaw control inputs, respectively. The fifth column states whether a particular combination should be considered in the constraint function. The sixth column gives a short motivation for the decision to include or exclude a particular combination. Each of the 26 combinations was considered, and when it was clear that a particular combination was unlikely to

occur within this UAVs typical mission profile, it was removed from the constraint function. Table 1 was then used to determine the command combinations that might result in control surface saturation, and each combination pair is discussed below.

Table 1 Input command combinations

Combinations	r_p	r_r	r_y	Required	Comment
1	-1	0	-1	×	Unlikely combination
2	-1	0	0	✓	Full down pitch command
3	-1	0	1	-	Unlikely combination
4	-1	1	-1	×	Unlikely combination
5	-1	1	0	-	Unlikely combination
6	-1	1	1	×	Unlikely combination
7	-1	-1	-1	×	Unlikely combination
8	-1	-1	0	-	Unlikely combination
9	-1	-1	1	×	Unlikely combination
10	0	0	-1	✓	Left yaw command
11	0	0	1	✓	Right yaw command
12	0	1	-1	✓	Right Roll + left yaw command
13	0	1	0	✓	Right roll command
14	0	1	1	✓	Roll + yaw command
15	0	-1	-1	✓	Left Roll + left yaw command
16	0	-1	0	✓	Left roll command
17	0	-1	1	✓	Left roll + right yaw command
18	1	0	-1	✓	Full up pitch + left yaw command
19	1	0	0	✓	Full up pitch command
20	1	0	1	✓	Full up pitch + right yaw command
21	1	1	-1	×	Unlikely combination
22	1	1	0	✓	Full up pitch + right roll command
23	1	1	1	×	Unlikely combination
24	1	-1	-1	×	Unlikely combination
25	1	-1	0	✓	Full up pitch + left roll command
26	1	-1	1	×	Unlikely combination

In the first nine lines in Table 1, only one realistic command combination was identified for inclusion in the inequality constraints. This was line 2: a full nose-down pitch command with no roll or yaw command. The first nine lines all correspond to full nose-down pitch combinations. Since this UAV would not be required to perform any aerobatic maneuvers, a scenario where a combination of full nose-down pitch together with roll or yaw, or both, would be required for either left or right commands was considered unlikely to occur. A combination that had to be included, however, was the full nose-down pitch command in line 2, since these constraints determine the maximum control surface deflections that correspond with maximum inputs. If this constraint was neglected, a full nose-down pitch command could result in some control surfaces deflecting more than the prescribed amounts.

All the left and right roll and yaw command combinations listed in lines 10 to 18 in Table 1 were considered as possible command combinations that should be included in the inequality constraints. Since this UAV had no vertical control surface, it was hard to determine how much yaw control might be required during roll commands to eliminate the adverse yaw, and therefore the roll and yaw combinations were all included, as it was not impossible that they could be encountered at some time during a given mission. Table 1 further indicates that a full pitch-up (line 21) and -down (line 2), a full roll left (line 18) and right (line 15), and a full yaw left (line 10) and right (line 11) were all selected for inclusion in the constraint functions.

The remaining lines in Table 1, lines 20 to 26, included the full nose-up pitch command case (line 21), which was selected for inclusion as it may represent a condition during launch and recovery, where large positive pitch inputs are often required. The combinations of full nose-up pitch command and roll, or full nose-up pitch command and yaw, were also considered, as they may be required when maneuvering the aircraft at high angles of attack. It was not deemed necessary to consider the combination of pitch up together with both full simultaneous roll and yaw commands, as these would almost never be encountered for the missions for which this type of UAV was designed.

Fourteen possible combinations remained and are indicated with a tick (✓) in Table 1, which meant that each control surface would require 14 constraints. The trim variables obtained from Phase 1 were very similar for the control surface pairs illustrated in Fig 2. A small offset in left and right variables was observed – this was due to the propeller torque that was also modelled in the simulation, and not due to a geometrical asymmetry. Since the bias values were small, it was possible to reduce the number of constraints by averaging the left and right offsets in the trim vector. Equations 12 to 15 provide a mathematical expression of the averaging.

$$T_{12} = \frac{1}{2}(T_1 + T_2) \tag{12}$$

$$T_{34} = \frac{1}{2}(T_3 + T_4) \tag{13}$$

$$T_{56} = \frac{1}{2}(T_5 + T_6) \tag{14}$$

$$T_{78} = \frac{1}{2}(T_7 + T_8) \tag{15}$$

Averaging the trim values reduced the number of inequality constraints from 112 (14 combinations x 8 control surface pairs) to 56 (14 combinations x 4 control surface pairs). The inequality constraints were obtained by substituting the 14 realistic command combinations into the mixing function in order to obtain the control surface positions in terms of the design variables. The final mixing function is expressed in Equation 16 below.

$$\begin{bmatrix}\delta_1\\ \delta_2\\ \delta_3\\ \delta_4\\ \delta_5\\ \delta_6\\ \delta_7\\ \delta_8\end{bmatrix} = \begin{bmatrix} x_1 & x_2 & x_3\\ x_1 & x_2 & x_3\\ x_4 & x_5 & x_6\\ x_4 & x_5 & x_6\\ x_7 & x_8 & x_9\\ x_7 & x_8 & x_9\\ x_{10} & x_{11} & x_{12}\\ x_{10} & x_{11} & x_{12}\end{bmatrix}\begin{bmatrix}{r_p}^2\\ {r_r}^2\\ {r_y}^2\end{bmatrix} + \begin{bmatrix} x_{13} & x_{14} & x_{15}\\ x_{13} & -x_{14} & -x_{15}\\ x_{16} & x_{17} & x_{18}\\ x_{16} & -x_{17} & -x_{18}\\ x_{19} & x_{20} & x_{21}\\ x_{19} & -x_{20} & -x_{21}\\ x_{22} & x_{23} & x_{24}\\ x_{22} & -x_{23} & -x_{24}\end{bmatrix}\begin{bmatrix}r_p\\ r_r\\ r_y\end{bmatrix} + \begin{bmatrix}T_{12}\\ T_{12}\\ T_{34}\\ T_{34}\\ T_{56}\\ T_{56}\\ T_{78}\\ T_{78}\end{bmatrix} \tag{16}$$

The inequality constraints derived from what was considered realistic command combinations were manipulated to take on the standard form used by most optimization programs. The approximate indication of maximum deflection that a control surface would experience during a typical flight is given by the term *k* in the equations below; this is typically 30° for this particular UAV – a physical limit due to the way that the control surfaces were actuated. Note that it is theoretically possible to use a different limit for each control surface. The inequality constraint terms were squared to remove the necessity of considering the positive and negative deflections as separate constraints. The inequality constraint pair for control surfaces 1 and 2 is expressed in equations 17 to 30.

$$g_1 = (x_3 - x_{15} + T_{12})^2 - k^2 \tag{17}$$

$$g_2 = (x_3 + x_{15} + T_{12})^2 - k^2 \tag{18}$$

$$g_3 = (x_2 + x_3 + x_{14} - x_{15} + T_{12})^2 - k^2 \quad (19)$$

$$g_4 = (x_2 + x_3 + x_{14} + x_{15} + T_{12})^2 - k^2 \quad (20)$$

$$g_5 = (x_2 + x_{14} + T_{12})^2 - k^2 \quad (21)$$

$$g_6 = (x_2 - x_{14} + T_{12})^2 - k^2 \quad (22)$$

$$g_7 = (x_2 + x_3 - x_{14} - x_{15} + T_{12})^2 - k^2 \quad (23)$$

$$g_8 = (x_2 + x_3 - x_{14} + x_{15} + T_{12})^2 - k^2 \quad (24)$$

$$g_9 = (x_1 + x_3 + x_{13} - x_{15} + T_{12})^2 - k^2 \quad (25)$$

$$g_{10} = (x_1 + x_3 + x_{13} + x_{15} + T_{12})^2 - k^2 \quad (26)$$

$$g_{11} = (x_1 + x_{13} + T_{12})^2 - k^2 \quad (27)$$

$$g_{12} = (x_1 - x_{13} + T_{12})^2 - k^2 \quad (28)$$

$$g_{13} = (x_1 + x_2 + x_{13} + x_{14} + T_{12})^2 - k^2 \quad (29)$$

$$g_{14} = (x_1 + x_2 + x_{13} - x_{14} + T_{12})^2 - k^2 \quad (30)$$

D. Normalization

The design variables were internally normalized by the optimization algorithms used in this project. However, the objective function terms had different units, which made it difficult to determine the optimal weights, and therefore normalization was required. The normalization process required four optimization runs, since each term in the objective function had to be normalized individually with its maximum achievable value. In order to obtain the maximum roll rate, for example, the simulation was run given a full right roll input command, while only the roll response was included in the objective (it was multiplied by -1, since it had to be maximized and the optimizer

expected a minimization problem). The remaining parameters were treated similarly. These runs were executed at the specific flight conditions of interest. The results presented in this paper represent the 40 m/s flight condition.

Table 2 Normalization runs

Run	Objective function
1	$f(\boldsymbol{x}) = \dot{p}_{\max}$
2	$f(\boldsymbol{x}) = \beta_{\min}$
3	$f(\boldsymbol{x}) = \dot{q}_{\max}$
4	$f(\boldsymbol{x}) = \dot{q}_{\min}$

Once the maximum rates and sideslip values had been obtained through the runs summarized in Table 2, the objective function was normalized using these values. The normalized objective function is illustrated in Equation 31, and a breakdown of the normalized terms is given in equations 32 to 35 below. Constraints may also have different units, similar to those of the objective functions. In that case, the constraint normalization method in [19] can be implemented. The constraints defined in this project, however, have the same units and did not require normalization.

$$f(x) = -(2w_1 f_1 + 2w_2 f_2 + w_3 f_3 + w_4 f_4) \tag{31}$$

$$f_1 = \frac{\dot{p}}{|\dot{p}_{\max}|} \tag{32}$$

$$f_2 = -\frac{\beta}{|\beta_{\min}|} \tag{33}$$

$$f_3 = \frac{\dot{q}_{pos}}{|\dot{q}_{\max}|} \tag{34}$$

$$f_4 = -\frac{\dot{q}_{neg}}{|\dot{q}_{\min}|} \tag{35}$$

IV. Results

The control allocation design methodology was implemented and evaluated at various flight conditions, although only the results of one flight condition are presented in this paper. It should be noted that the purpose of this work was not to find the most efficient optimization algorithm for this design problem. Several optimization algorithms could have been used, but since the responses (used in the objective function and the equality constraints), the

design variables and the inequality constraints were all smooth, continuous, differentiable functions, it was possible to utilize gradient based methods that are generally faster for this type of problem than population based methods. In particular, a leapfrog and a sequential quadratic programming (SQP) method were evaluated, which were both capable of nonlinear optimization with linear or nonlinear constraints. The control allocation results are given in the first section, followed by the optimization results. The results presented below were conducted for a typical high-speed flight condition for this particular UAV, which consisted of an airspeed of 40 m/s using a baseline set of weights all equal to 1. The impact of relative weightings was investigated and is discussed in the last section of the results. The optimization results for Phase 1 are given in Table 3 and the optimization results for Phase 2 are given in Table 4. The indirect function evaluations are those that involved the finite difference computations in gradient calculations. Both the leapfrog and the SQP method converged to the same final results (albeit slower in the case of the leapfrog method).

Table 3 Optimization overview for Phase 1

Total function evaluations	751
Direct function evaluations	451
Indirect function evaluation	300
Iterations	25
Optimization algorithm	SQP

Table 4 Optimization overview for Phase 2

Total function evaluations	1979
Direct function evaluations	635
Indirect function evaluation	1344
Iterations	1863
Optimization algorithm	SQP

The trim bias vector resulting from Phase 1 is given in Equation (36). The maximum deflection that a control surface could be deflected was 30° for this UAV. As can be seen in Equation (36) a maximum of 7.53% of the maximum control surface deflection was required to trim the aircraft. The asymmetric terms for the corresponding control surfaces observed in the trim bias vector were used by the optimizer to compensate for the propeller gyroscopic effects.

$$\boldsymbol{T} = \begin{bmatrix} 0.2674 \\ 0.6345 \\ -1.9112 \\ -1.2623 \\ -2.2601 \\ -1.9677 \\ 1.8300 \\ 1.9244 \end{bmatrix} \tag{36}$$

A. Control allocation

The optimal mixing values for the coefficient matrices $\boldsymbol{A}$ and $\boldsymbol{B}$ of Configuration 3 are given in Equation (37). The control allocation plots for the pitch, roll and yaw command ranges are illustrated in the figures below.

$$\begin{bmatrix} \delta_1 \\ \delta_2 \\ \delta_3 \\ \delta_4 \\ \delta_5 \\ \delta_6 \\ \delta_7 \\ \delta_8 \end{bmatrix} = \begin{bmatrix} -8.5337 & 6.6917 & -7.1426 \\ -8.5337 & 6.6917 & -7.1426 \\ 8.6901 & -2.9179 & 0.1430 \\ 8.6901 & -2.9179 & 0.1430 \\ 3.7301 & -3.2261 & 4.1580 \\ 3.7301 & -3.2261 & 4.1580 \\ -8.9079 & -8.9079 & 7.0307 \\ -8.9079 & -8.9079 & 7.0307 \end{bmatrix} \begin{bmatrix} {r_p}^2 \\ {r_r}^2 \\ {r_y}^2 \end{bmatrix} + \begin{bmatrix} 21.9172 & 6.6917 & -23.3083 \\ 21.9172 & -6.6917 & 23.3083 \\ -22.8967 & 11.2887 & 14.3496 \\ -22.8967 & -11.2887 & -14.3496 \\ -28.3838 & 0.0063 & -7.3904 \\ -28.3838 & -0.0063 & 7.3904 \\ 22.9693 & 22.9693 & -7.0307 \\ 22.9693 & -22.9693 & 7.0307 \end{bmatrix} \begin{bmatrix} r_p \\ r_r \\ r_y \end{bmatrix} + \begin{bmatrix} 0.2674 \\ 0.6345 \\ -1.9112 \\ -1.2623 \\ -2.2601 \\ -1.9677 \\ 1.8300 \\ 1.9244 \end{bmatrix} \tag{37}$$

Fig 4 presents the control surface positions resulting from a range of pitch commands from a full nose-down pitch command on the left to a full nose-up pitch command on the right. The aircraft figures on either side of the control allocation graph illustrate where the respective control surfaces were situated on the UAV. The arrows show whether the respective control surfaces were moving up or down for the given input command. In the case of a full nose-down pitch command, it can be seen that the control surfaces were all deflected to the maximum allowable value, while optimizer primarily allocated control surfaces 5 and 6 to be responsible for positive pitch control.

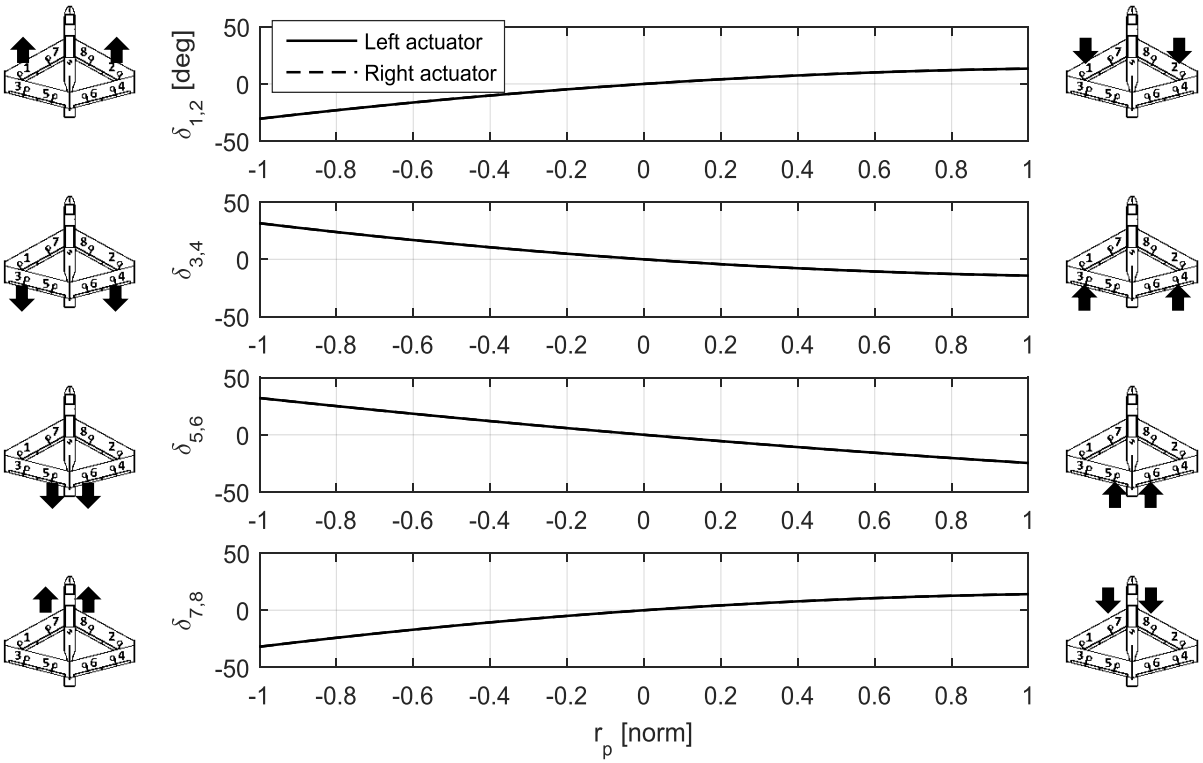

Fig 4 Control surface deflection for a nose-up pitching command

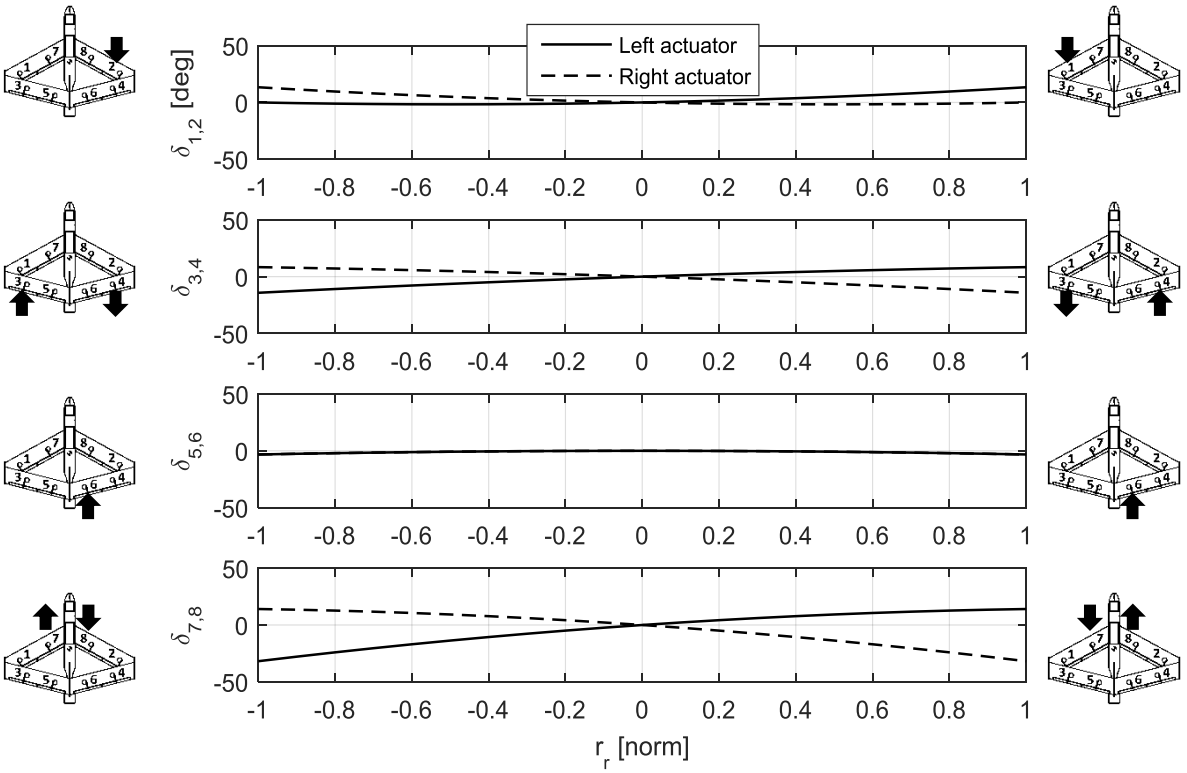

Fig 5 Roll command control allocation

The control allocation plot for the roll command range is illustrated in Fig 5. The control deflections for a full left-roll command ($r_r = -1$) is illustrated on the left and the control deflections for a full right-roll command ($r_r = 1$) is illustrated on the right. Fig 5 shows that control surfaces 1, 2, 3, 4, 7 and 8 were primarily used when a roll input command was given, since the optimizer reserved control surfaces 5 and 6 mainly for pitch control.

Fig 6 illustrates the control allocation for a range of yaw control input commands. The control deflections for a full nose-left yaw command ($r_y = -1$) is illustrated on the left and the control allocation for a full nose-right yaw command ($r_y = 1$) is illustrated on the right. As shown in Fig 6, the yaw control mixing was relatively complex and would have been difficult to design manually, since the optimizer utilized all the available control surfaces. Control surfaces 1, 2, 3 and 4 were primarily used for yaw control. A fairly small amount of control deflection was required from control surfaces 5 and 6, and 7 and 8 for yaw control.

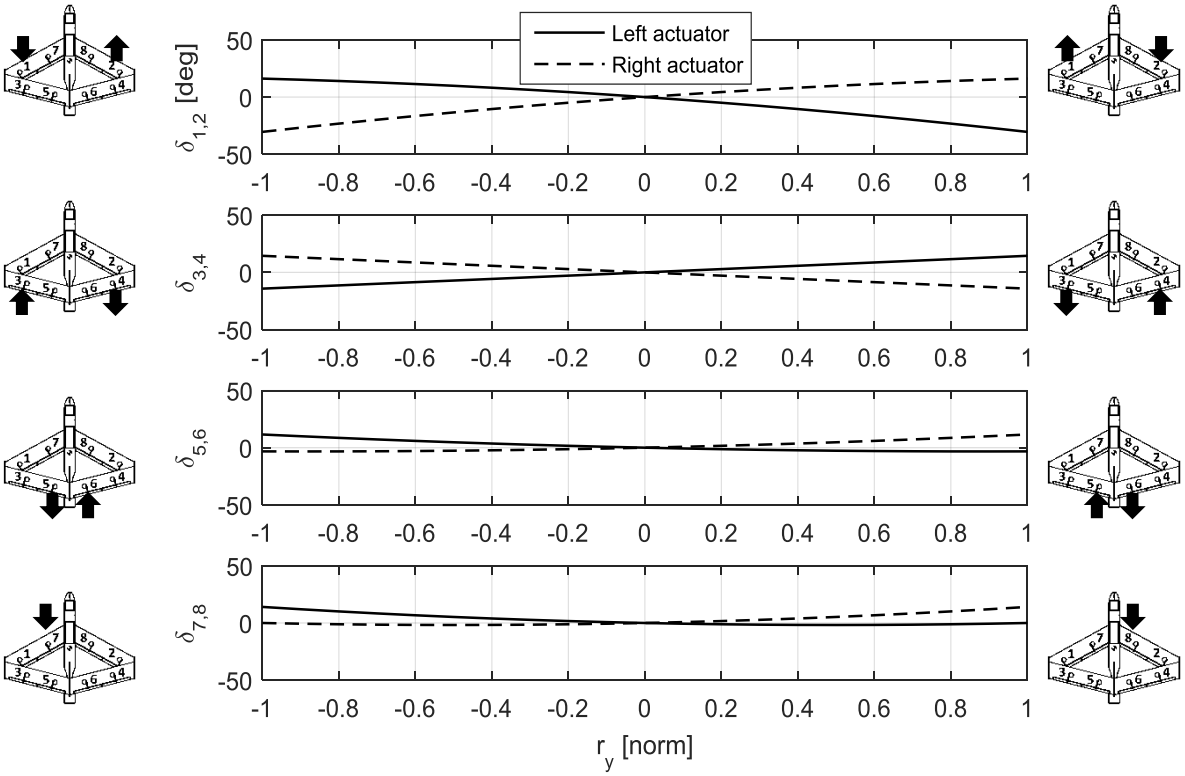

Fig 6 Yaw command control allocation

B. Objective function

The optimal accelerations and optimal sideslip corresponding to the objective function terms obtained at this flight condition are shown in Table 5. The maximum roll acceleration was obtained for a roll step input command,

the maximum sideslip was obtained for a yaw step input command and the maximum positive and negative pitch accelerations were obtained for a nose-up and nose-down step input command respectively.

Table 5 Objective function final solution

$\dot{p}\ [°/s^2]$	88.2
$\beta\ [°]$	-1.16
$\dot{q}_{pos}[°/s^2]$	45.5
$\dot{q}_{neg}[°/s^2]$	-77.6
$F(\boldsymbol{x}^*)$	-3.75

C. Constraints

The six equality constraints for Phase 1 and the four equality constraints for Phase 2 were all satisfied at the solution (within a very small tolerance), which was a partial confirmation of convergence. The inequality constraint results at the solution are given in Table 6, and the inequality constraints that were active at the optimum point are highlighted in the table.

Table 6 Inequality constraint results at the solution

g_1 = -623.9	g_{15} = -650.6	g_{29} = -810.9	g_{43} = -645.9
g_2 = 0.000	g_{16} = -733.4	g_{30} = -871.4	g_{43} = -896.5
g_3 = -0.000	g_{17} = -844.9	g_{31} = -861.4	g_{44} = 0.000
g_4 = -623.9	g_{18} = -447.3	g_{32} = -826.6	g_{46} = -645.9
g_5 = -708.6	g_{19} = -853.9	g_{33} = -871.6	g_{47} = -645.9
g_6 = -899.8	g_{20} = -650.6	g_{34} = -871.4	g_{48} = 0.000
g_7 = -623.9	g_{21} = 0.000	g_{35} = -861.5	g_{49} = -645.9
g_8 = -0.000	g_{22} = -898.3	g_{36} = -826.4	g_{50} = -0.000
g_9 = 0.000	g_{23} = -0.000	g_{37} = -668.4	g_{51} = -0.000
g_{10} = -623.9	g_{24} = -898.3	g_{38} = 0.000	g_{52} = -645.9
g_{11} = -708.6	g_{25} = -650.6	g_{39} = -183.5	g_{53} = -645.9
g_{12} = -0.000	g_{26} = -0.000	g_{40} = -0.000	g_{54} = -0.000
g_{13} = -159.2	g_{27} = -844.9	g_{41} = -0.758	g_{55} = -0.000
g_{14} = -708.6	g_{28} = 0.000	g_{42} = 0.000	g_{56} = -645.9

The active inequality constraints for the respective control surface pairs are given in Table 7. The first column in Table 7 represents the inequality constraints that were active at the optimum point. The control command combinations corresponding to these active constraints are given in the next three columns, together with a short description of the corresponding commands in the last column.

Table 7 Active inequality constraints

Active inequality constraints for control surface 1 and 2				
# g(x)	r_p	r_r	r_y	**Comment**
2	0	0	1	Right-yaw command
3	0	1	-1	Roll + yaw command
8	0	-1	1	Roll + yaw command
9	1	0	-1	Positive pitch + yaw command
12	-1	0	0	Negative pitch command
Active inequality constraints for control surface 3 and 4				
# g(x)	r_p	r_r	r_y	**Comment**
21	0	-1	-1	Roll + yaw command
23	1	0	-1	Pitch + yaw command
26	-1	0	0	Negative pitch command
28	1	-1	0	Pitch + roll command
Active inequality constraints for control surface 5 and 6				
# g(x)	r_p	r_r	r_y	**Comment**
38	1	0	1	Positive pitch + yaw command
40	-1	0	0	Negative pitch command
42	1	-1	0	Pitch + roll command
Active inequality constraints for control surface 7 and 8				
# g(x)	r_p	r_r	r_y	**Comment**
45	0	1	-1	Roll + yaw command
48	0	-1	0	Left-roll command
50	0	-1	1	Roll + yaw command
51	1	0	-1	Pitch + yaw command
54	-1	0	0	Negative pitch command
55	1	1	0	Pitch + roll command

D. Simulated aircraft response

The aircraft dynamic responses were simulated to demonstrate the results for a full roll and yaw command using the optimized control allocation function. The aircraft lateral response for a pure roll command is illustrated in Fig 7. A steady roll rate of 70°/s was reached within 0.1 seconds after the control input was given. Very little rudder control was needed to coordinate the aircraft for the small sideslip and lateral acceleration generated during a roll maneuver.

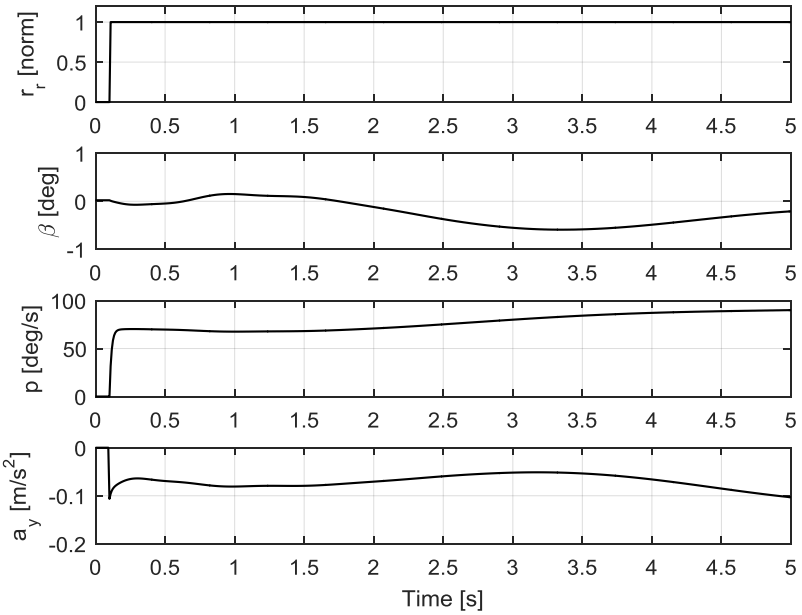

Fig 7 Dynamic response for a pure roll input command

The aircraft lateral response for a pure yaw command for Configuration 3 is illustrated in Fig 8. The controls were not particularly effective to yaw the aircraft, since a maximum yaw input was only able to generate an approximate steady-state sideslip angle of -2°. There was no initial roll response to a yaw input. The longer-term roll response to a yaw input was caused by the dihedral effect. The yaw rate slowly increased after 1.7 seconds.

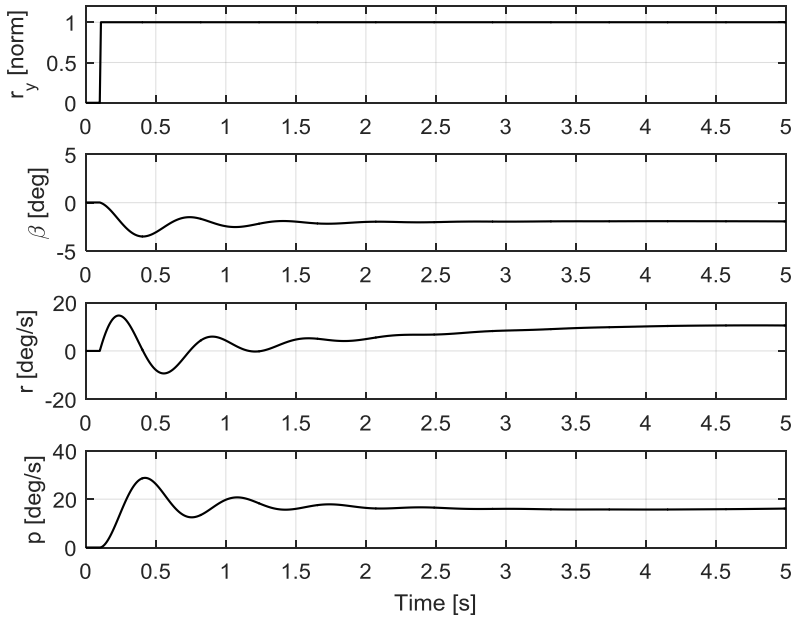

Fig 8 Dynamic response for a pure yaw input command

E. Off design performance

The amount of pitch input command required to trim the UAV over the entire flight envelope is shown in the figure below. The solid circle in Fig 9 represents the condition at which the control allocation function was designed. Fig 9 shows that a maximum of 63% input command at low speed was required to trim the aircraft. A sufficient control surface deflection margin remained for low speeds, which was desired. An adequate amount of control authority therefore remains to trim the aircraft throughout the speed envelope.

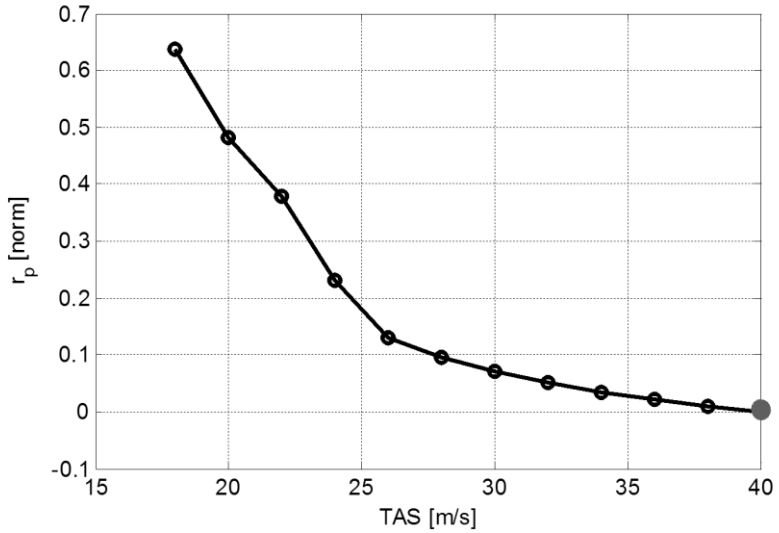

Fig 9 Pitch authority required to trim the UAV over the flight envelope

F. Impact of relative weightings

The impact of the relative objective function term weightings was investigated using the results given above as a baseline. The goal was to determine whether the expected outcome would be obtained if the weights were adjusted intuitively to meet the desired requirements according to the methodology discussed in the paper. The baseline weights, together with the adjusted weights, are reflected in Table 8 below. This table show that the nose-up pitch rate and sideslip objective weights were increased to emphasize their importance, and the roll rate and nose-down pitching moment weights remained unchanged.

Table 8 Baseline and adjusted weights for a flight condition of 40 m/s

	w_1	w_2	w_3	w_4
Baseline weights	1.0	1.0	1.0	1.0
Adjusted weights	1.0	1.2	1.5	1.0

A comparison between the baseline and adjusted weights, based on the amount of pitch command to trim the aircraft, is provided in Fig 10. The weight for the nose-up pitching moment was increased, and it can be seen that less pitch command was required to trim the aircraft at airspeeds between 18 and 22 m/s, as desired and as expected from the adjusted weights.

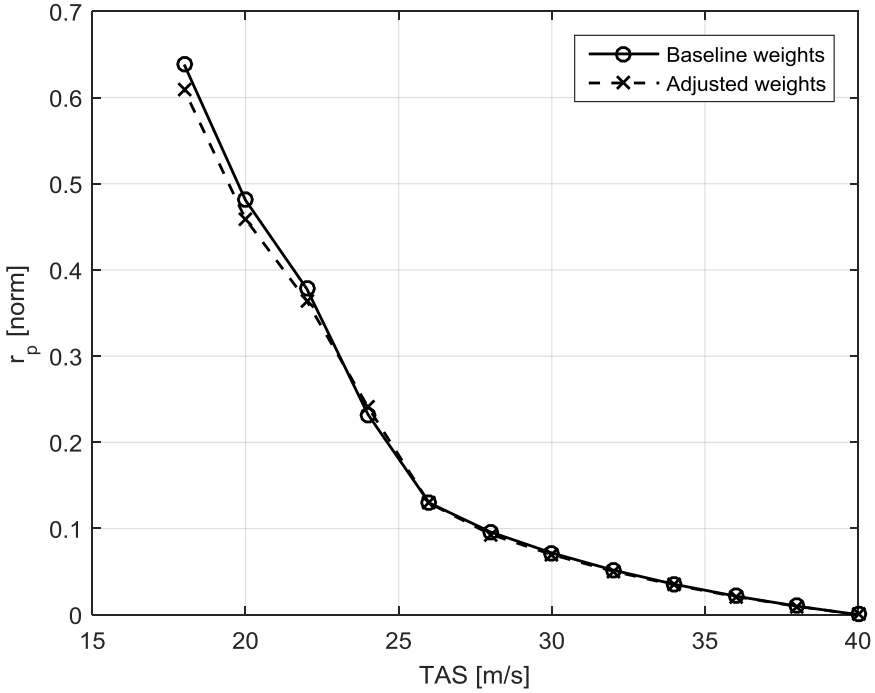

Fig 10 Pitch authority required to trim the UAV, comparing baseline and adjusted weights

The response to a full right rudder command is illustrated in Fig 11. It was expected that a slightly bigger sideslip would be generated for the adjusted weight, as the sideslip term weight in the objective function was increased. A noticeable difference in the sideslips was seen – a larger sideslip was generated using the adjusted weight configuration, as desired.

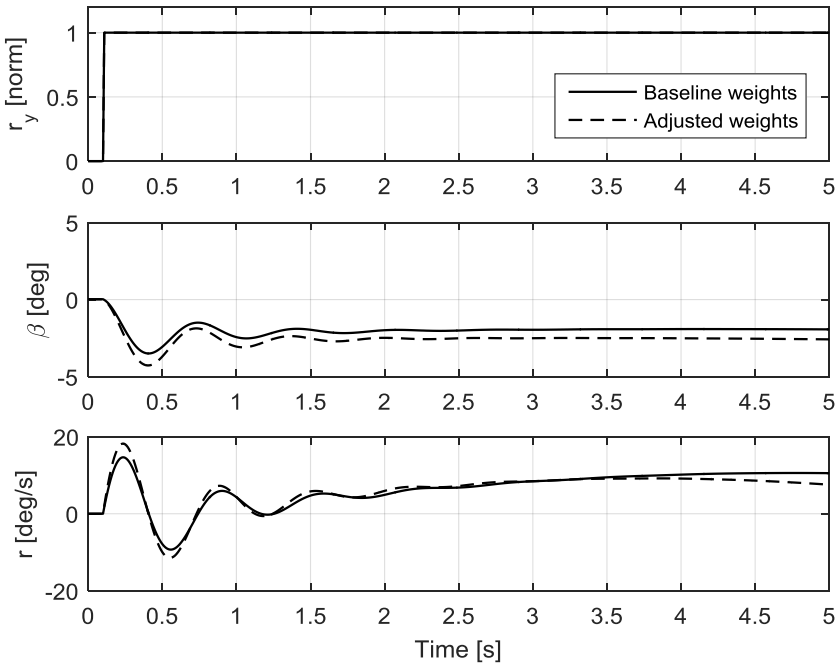

Fig 11 Dynamic response for a pure yaw input, comparing baseline and adjusted weights

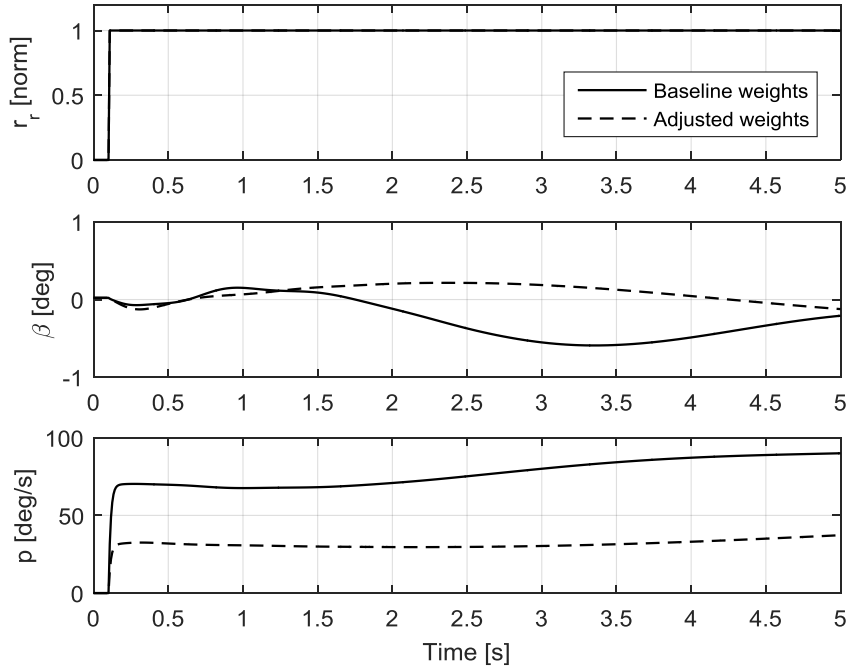

Fig 12 Dynamic response for a pure roll input, comparing baseline and adjusted weights

A full right-roll command is illustrated in Fig 12. The initial sideslip generated for the two configurations were similar, but after 0.1 seconds, the two configurations produced different results. The roll rate generated for the adjusted weight configuration was significantly less than that for the baseline case. This result is due to the increased

weights on the other terms, which the optimizer exploited by reducing the amount of control surface deflections assigned to roll control.

In summary, the aircraft response to the individual control commands can easily be tailored by adjusting the weights in the objective function. This adjustment can be performed intuitively. Although more sophisticated multi-objective techniques, such as computing the Pareto front, could be utilized, it was not considered necessary in order to utilize the current technique in a practical design problem.

V. Conclusion

This paper presented an open-loop control allocation methodology for unconventional aircraft using mathematical optimization techniques. The primary goal was to design an open-loop control allocation program that could be utilized during initial flight testing, as a backup mode following a failure anywhere within the feedback system, or to simplify the inner loops of a closed-loop control or stability augmentation design. The control allocation method consisted of mapping conventional input commands such as pitch, roll and yaw, to the individual control surfaces in order to achieve an open-loop response similar to that of a conventional aircraft.

The control allocation design method made use of multiple-objective constrained optimization. A second-order mixing function was selected to perform the control allocation. This mixing function consisted of a constant term, a linear term and a quadratic term, which gave the optimizer considerable flexibility in assigning the control surfaces. The constant term was utilized to satisfy the steady-state trim condition, and the linear and quadratic terms were used to obtain optimal control mixing for maneuvering, control and trim at other flight conditions. The methodology was demonstrated using a Rhomboid-wing UAV implemented in a high fidelity simulation environment, the resulting aircraft response was demonstrated to be conventional and satisfactory, with enough authority to control a typical UAV in manual or automated flight. All the design requirements were met, and it was demonstrated how the response could be tailored intuitively by adjusting the weights in the objective function.

Acknowledgments

The authors would like to thank the Aerospace Industry Support Initiative (AISI) in South Africa that funded and supported this project. The authors would also like to thank Paramount Advanced Technologies (PAT) for providing the UAV and the related design data.

References

[1] Wolkovitch, J., "Joined wing aircraft", United States of America Patent 4,365,773, 28 December 1982.

[2] Schiktanz, D. and Scholz, D., "Box Wing Fundamentals - An Aircraft Design Perspective", *Proceedings of the Deutscher luft- und Raumfahrtkongress (DGLR) Conference*, Bremen, DEU, 2011.

[3] Jemitola, P. O. and Fielding, J. P., "Box Wing Aircraft Conceptual Design", *Proceedings of the 28th International Council of the Aeronautical Science (ICAS) Congress*, Brisbane, AU, 2012.

[4] Corneille, J., "Wind Tunnel Investigation Of Joined Wing Configurations", MEng Thesis, Air Force Institute of Technology, Fairborn, OH, 1999.

[5] Zafirov, D., "Closed Wing Aircraft Classification", *International Journal of Engineering Research & Technology*, vol. 3, no. 1, pp. 10-15, 2014.

[6] Kroo, I., McMasters, J. and Smith, S. C., "Highly Nonplanar Lifting Systems", Presented at: Transportation Beyond 2000: Technologies Needed for Engineering Design NASA Langley Research Center, September 26-28, 1995.

[7] Zhang, Y., Suresh, S. V., Jiang, B., and Theilliol, D., "Reconfigurable Control Allocation against Aircraft Control Effector Failure", *Proceedings of the Institute of Electrical and Electronics Engineers (IEEE) International Conference on Control Applications*, Singapore, 2007.

[8] Poonamallee, V. L., Yurkovich, S., Serrani, A., Doman, D. B., and Oppenheimer, M. W., "A Nonlinear Programming Approach for Control Allocation", *Proceedings of the American Control Conference*, Boston, MA, 2004.

[9] Oppenheimer, M. W., and Doman, D. B., "Control allocation for overactuated systems", Air Force Research Laboratory, AFRL-VA-WP-TP-2006-321, Fairborn, OH, 2006.

[10] Basson, L., "Control allocation as part of a fault-tolerant control architecture for UAV's", MSc Thesis, Department of Electrical and Electronic Engineering, Stellenbosch University, South Africa, 2011.

[11] Davidson, J. B., Lallman, F. J., and Bundick, T. W., "Real-Time Adaptive Control Allocation applied to a High Performance Aircraft", *Proceedings of the 2001 5th Society for Industrial and Applied Mathematics (SIAM) Conference on Control & Its Applications, San Diego, CA*, 2001.

[12] Wu, S. F., Engelen, C. J., Chu, Q. P., Babuska, R., Mulder, J. A. and Ortega, G., "Fuzzy logic based attitude control of the spacecraft X-38 along a nominal re-entry tragectory", *Control Engineering Practice*, no. 9, pp. 699-707, 2001.

[13] Burden, R. L. and Faires, J. D., "Numerical Analysis", 9th ed., Richard Stratton, Canada, 2011.

[14] Skinner, P., "Low-speed Wind Tunnel Test of the Roadrunner Joined Wing Configuration", DPSS-ASC2014/054, Council for Scientific and Industrial Research, Pretoria, South Africa, 2014.

[15] DeLoach, R., "Application of Modern Experiment Design to Wind Tunnel Testing at NASA Langley Research Centre", *Proceedings of the 36th AIAA Aerospace Sciences Meeting and Exhibit, Reno, NV*, vol. 0713, p. 98, 1998.

[16] Giunta, A., Wojtkiewicz, S. J. and Eldred, M., "Overview of Modern Design of Experiments Methods for Computational Simulations", *Proceedings of the 41st AIAA Aerospace Sciences Meeting and Exhibit, Reno, NV*, vol. 0649, 2003.

[17] Drela, M., Youngren, H., "AVL (Athena Vortex LAttice)" [Online], 2004, http://web.mit.edu/drela/Public/web/avl [retrieved 7 January 2014].

[18] Stevens, B. L., and Lewis, F. L., “Aircraft control and simulation”, 2nd ed., Wiley, Hoboken, New Jersey, 2003.

[19] Arora, J. S., “Introduction to optimum design”, 3rd ed., Elsevier, Atlanta, Georgia, 2012.